DOI 10.4430/bgo00428

New methodological approach in the evaluation of fault interaction: insights from the central Apennines fault system

G. Valentini[1,2], T. Volatili[1], P. Galli[3,4] and E. Tondi[1,2]

[1] *School of Science and Technology, Geology Division, University of Camerino, Camerino, Italy*
[2] *Istituto Nazionale di Geofisica e Vulcanologia, Sezione di Sismologia e Tettonofisica, Camerino, Italy*
[3] *Dipartimento Protezione Civile, Roma, Italy*
[4] *Consiglio Nazionale delle Ricerche, Istituto di Geologia Ambientale e Geoingegneria, Roma, Italy*

(Received: 23 November 2022; accepted: 12 July 2023; 26 September 2023)

ABSTRACT The central Apennines host several normal active faults, which are distributed along the Central Apennine Fault System (CAFS), known for generating dozens of earthquakes, of moderate to high magnitudes, in the last thousand years. The latest events caused by this system occurred in the epicentral area of Colfiorito in 1997 (M_w 6.0), L'Aquila in 2009 (M_w 6.2), and at the border between the Marche, Umbria, and Lazio regions in 2016 (M_w 6.6), this latter a catastrophic event with hundreds of victims and extensive damages. Thereafter, significant interest arose in the study of fault behaviour in the axial zone of the central Apennines. This work proposes a new methodological approach to studying fault interaction within the framework of the CAFS seismic cycle, modelling faults with a more complex geometry characterised by an elliptical outline, which better describes the actual shape of a fault at depth. All the destructive earthquakes ($M_w > 6.0$) that occurred in the last thousand years were taken into account, and the static stress between the causative fault and adjacent one was calculated. The results demonstrate how the newly modelled faults critically affect Coulomb stress transfer compared to planar and rectangular fault modelling usually adopted by previous authors.

Key words: active normal faults interaction, Coulomb stress transfer, fault modelling, seismic cycle, Central Apennines Fault System.

1. Introduction

The Central Apennines Fault System [CAFS in Cello *et al*. (1997)] is composed of several active normal to oblique faults that have caused several destructive earthquakes during the last millennium. According to seismic catalogues [CPTI15: Rovida *et al*. (2022)], 15 seismic events with $5.8 \leq M_w \leq 7.0$ in central Italy (since 1279) can be associated with CAFS-related structures. Seismicity appears to be concentrated in three distinct time windows: in the 12th-13th centuries, in the 17th-18th centuries, and between the end of the 20th century to the present day. The most recent seismic events struck the axial zone of the central Apennine fold-thrust belt between 1979 (the M_w 5.8 Valnerina sequence) and 2016-2017 [the M_w 6.5 Amatrice-Norcia-Visso sequence: Chiaraluce *et al*. (2017)]. They also involved the northern area of the CAFS and

its southern border [1997, the M_w 6.0 Colfiorito-Sellano and 2009, M_w 6.2 L'Aquila sequences, respectively: Amato *et al*. (1998), Cello *et al*. (1998), Tondi (2000), Vittori *et al*. (2000), Chiarabba *et al*. (2009), Chiaraluce *et al*. (2011), Pantosti and Boncio (2012), Vannoli *et al*. (2012), and references therein], causing severe damage and hundreds of casualties, and thus prompting greater interest in the study of the seismic behaviour of these seismogenic structures.

The Apennines host the CAFS in their central portion, extending 100 km in a NW-SE direction, and 50 km from west to east. In this system, several segmented surface expressions of seismogenic sources outcrop, and have been precisely mapped (Barchi *et al*., 2000; Galadini and Galli, 2000; Tondi, 2000; Tondi *et al*., 2020). Furthermore, numerous paleoseimological analyses (Galli *et al*., 2008, 2022a, 2022b; Galli, 2020), conducted on trenches along faults, have provided useful information on their past activity.

Today, one of the main research objectives in the field of earthquake geology is to understand the mechanisms that influence recurrence intervals. By studying the interaction between neighbouring faults, it is possible to estimate which fault is the most prone to slip. Although several factors can influence fault activity, such as fluid circulation, climate-controlled changes in surface loads or elastic strain energy accumulation (Hetzel and Hampel, 2005; Oskin *et al*., 2008; Brodsky and van der Elst, 2014; Gold *et al*., 2017; Wedmore *et al*., 2017), static and dynamic stress transfers play a crucial role in triggering fault ruptures. In particular, the rapid propagation of seismic waves produces short-term changes in dynamic stress, whereas static stress transfer is a permanent variation of the stress condition in the crust around a causative fault, also affecting faults far from the source (Gomberg and Johnson, 2005; Velasco *et al*., 2008; Toda *et al*., 2012). Since we are investigating stress transfer over an entire millennium, static Coulomb stress transfer (CST) within the CAFS is of primary importance.

In this study, we reconstructed the CAFS seismic cycle (Tondi and Cello, 2003) by considering the three time windows of seismicity over the last millennium, and investigated the role of CST in promoting or inhibiting the ruptures of neighbouring faults (Fig. 1b). Furthermore, considering the importance of fault geometry in influencing the result, we propose a new strike-variable and ellipse-shaped 3D model as input for the CST simulations.

1.1. The Central Apennine Fault System (CAFS)

The Italian central Apennines are dissected by several NW–SE-trending normal-to-oblique faults developed coherently with the current extensional regional stress field. Since the Late Quaternary, the central Apennines have been subject to a NE–SW-oriented minimum horizontal compressive stress producing large sub-parallel extensional faults that, in some cases, overlaid on older compressive structures inverting the kinematic consistency with the formation of the fold-thrust belt (Cello *et al*., 1997). This structural framework accounts for surface evidence of normal faulting along a very large area, extending from Colfiorito (the CAFS northern edge) to L'Aquila, usually bordering the eastern side of tectonic basins infilled by Pleistocene to Holocene deposits. The slickensides, outcropping in almost the entire CAFS, show signs of recent fault activity, often by displaying kinematic indicators consistent with the current stress field. According to the empirical relationship between length and magnitude proposed by Galli *et al*. (2008), the expected magnitude of the CAFS faults varies within a range from M_w 5.7 to M_w 7.0. The surface length of the faults ranges from a few kilometres up to 44 km [e.g. the Gran Sasso fault: Galli *et al*. (2022a)], with an average dip angle of approximately 57°. In recent decades, the CAFS has been extensively studied by several authors, and the fault scarps have been mapped in detail, thus providing valuable data for seismic hazard assessment. For the purpose of modelling,

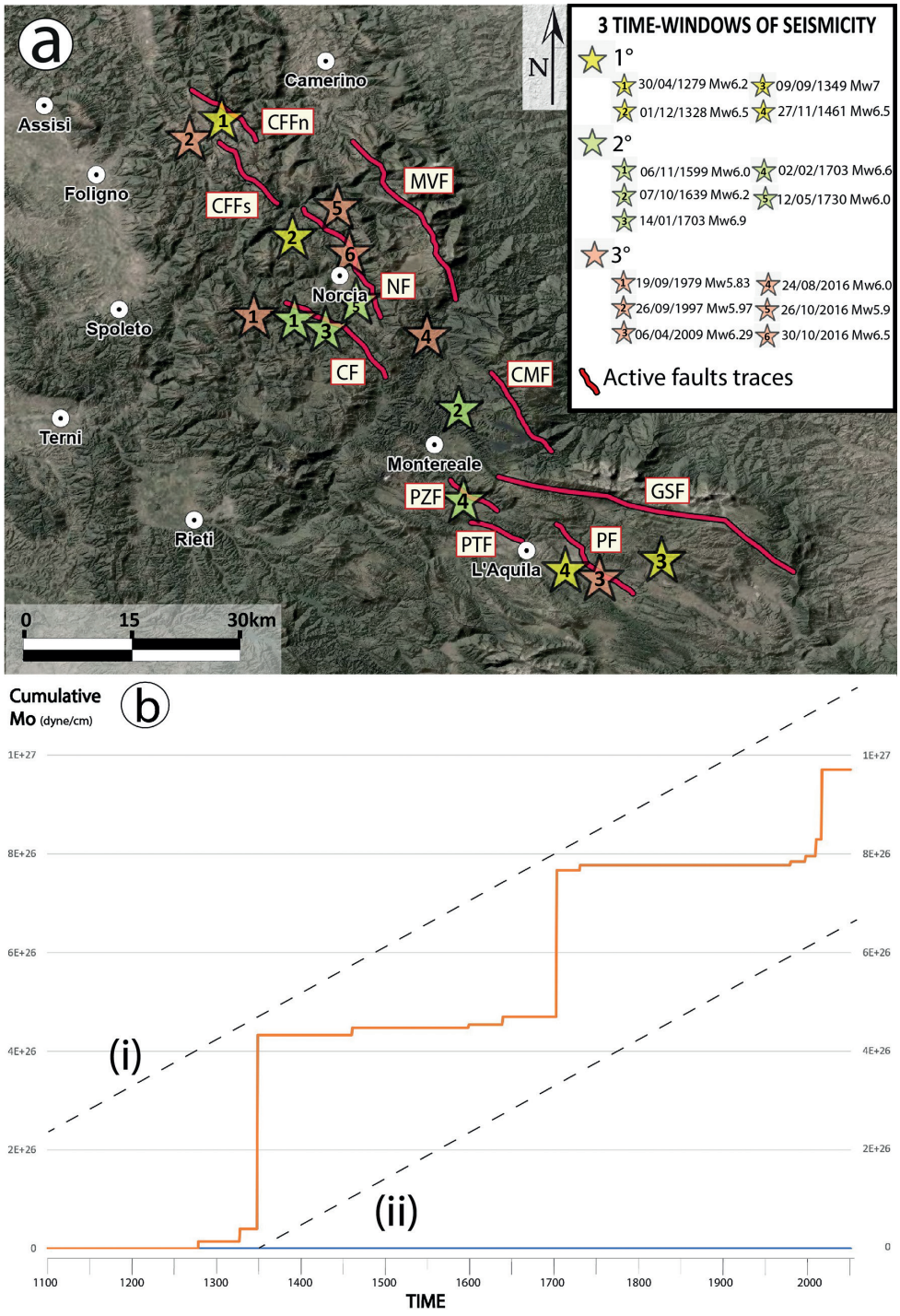

Fig. 1 - a) Map of the 15 seismic events with 5.8 ≤ M_w ≤ 7.0 in the CAFS area since 1279. Main active fault traces on the topographic surface are also shown in red (CFFn - Colfiorito North fault; CFFs - Colfiorito South fault; MVF - Mount Vettore fault; NF - Norcia fault; CF - Cascia fault; CMF - Campotosto fault; GSF - Gran Sasso fault; PZF - Pizzoli fault; PF - Paganica fault; PTF - Pettino fault) (Tondi, 2000; Galderisi and Galli, 2020; Tondi *et al*., 2020; Galli *et al*., 2022a, 2022b; and references therein). b) CAFS cumulative seismic moment (dyne/cm) as a function of time. Dashed lines show the hypothetical course of the seismic cycle if the system had been: i) energy-predictable and ii) time-predictable (Shimazaki and Nakata, 1980; Tondi and Cello, 2003).

only the main fault traces associated to the studied seismogenic sources have been considered in this work, although the superficial expression of these deep seismogenic structures may be represented by multiple surface ruptures. These structures generated several large earthquakes over the last thousand years, as recorded by the Italian historical catalogues, which are among the most complete and furthest back-in-time seismic compilations worldwide. Historical data, supported by hundreds of paleoseismological surveys, enabled acquiring a large amount of reliable data on the recent activity of the CAFS.

2. Methods

2.1. Seismic data and causative faults

In this study, a total of 15 earthquakes have been considered, and their parameters summarised in Table 1. Specifically, nine historical earthquakes [CPTI15 seismic catalogue (Rovida *et al.*, 2022)] and six instrumental ones (ISIDe Working Group, 2007; https://doi.org/10.13127/ISIDE), with $M_w \geq 6.0$ and $M_w \geq 5.8$, respectively, have been selected. Different magnitude thresholds for historical and instrumentals data sets were adopted to overcome the probable overestimation of the estimated magnitude for historical events (Vannucci *et al*., 2021 and references therein). Once all the historical earthquakes were selected based on magnitude, an additional strategy was adopted to overcome the overestimation issue: the catalogues provide an error for each magnitude, and for calculation purposes, the error was subtracted from the magnitude indicated in the catalogue. For the 1349 seismic event, the data in the catalogue have been replaced with the recent revision by Galli *et al*. (2022a), who identified the source of this devastating earthquake and attributed an $M_w = 7$.

A causative fault has been associated with each earthquake studied after examining in detail fault-related data present in literature (i.e. paleoseismological, structural, macroseismic).

Table 1 - List of historical ($M_w \geq 6.0$) and instrumental ($M_w \geq 5.8$) seismic events from 1279 to 2016, caused by the CAFS [from CPTI15: Rovida *et al*. (2022) and ISIDe seismic catalogues: ISIDe Working Group (2007), https://doi.org/10.13127/ISIDE]. TM_w = type of M_w: Mdm = macroseismic from intensity data; InsO = instrumental.

Year	Month	Day	Epicentral area	Lat	Lon	Io	M_w	Error M_w	TM_w	Source
1279	4	30	Umbria-Marche Apennines	43.093	12.872	9	6.20	0.16	Mdm	CPTI15
1328	12	4	Valnerina	42.857	13.018	10	6.49	0.28	Mdm	CPTI15
1349	9	9	Abruzzo	42.334	13.613	10	7.00	ND	Mdm	Galli *et al.*, 2022
1461	11	27	L'Aquila	42.308	13.543	10	6.50	0.46	Mdm	CPTI15
1599	11	6	Valnerina	42.724	13.021	9	6.07	0.24	Mdm	CPTI15
1639	10	7	Laga Mountains	42.639	13.261	9-10	6.21	0.15	Mdm	CPTI15
1703	1	14	Valnerina	42.708	13.071	11	6.92	0.1	Mdm	CPTI15
1703	2	2	L'Aquila	42.434	13.292	10	6.67	0.11	Mdm	CPTI15
1730	5	12	Valnerina	42.753	13.120	9	6.04	0.1	Mdm	CPTI15
1979	9	19	Valnerina	42.73	12.956	8-9	5.83	0.1	InsO	CPTI15
1997	9	26	Umbria-Marche Apennines	43.014	12.853	8-9	5.97	0.07	InsO	CPTI15/ISIDe
2009	4	6	L'Aquila	42.309	13.510	9-10	6.29	0.07	InsO	CPTI15/ISIDe
2016	8	24	Laga Mountains	42.698	13.233	10	6.00	0.07	InsO	CPTI15/ISIDe
2016	10	26	Valnerina	42.904	13.090		5.90	0.07	InsO	CPTI15/ISIDe
2016	10	30	Valnerina	42.83	13.109	11	6.50	0.07	InsO	CPTI15/ISIDe

Next, the causative fault trace was processed in a Geographic Information System (GIS, refer to Fig. 1a), with a resolution based on the CAFS scale. All the constructed lineaments are supported by robust field-based constraints from literature (Galli and Galadini, 1999; Tondi, 2000; Galadini and Messina, 2001; Messina *et al*., 2002; Tondi and Cello, 2003; Galli *et al*., 2005, 2011, 2016, 2018, 2019a, 2019b, 2022a, 2022b; Galderisi and Galli, 2020; Tondi *et al*., 2020, and references therein). The fault data set was compiled with the following fields: i) fault name, ii) dip angle, iii) rake [using the Aki and Richards (1980) conventions], iv) dip direction, and v) length.

We estimated the seismic moment released by historical earthquakes by extrapolating it from the Hanks and Kanamori (1979) formula. The following equation was applied:

$$M_0 = 10^{\left(\frac{3}{2}\right) \times (M_W + 10.73)} \quad (1)$$

where M_0 is the seismic moment and M_W is the moment magnitude. Next, we compared the seismic energy released during the main seismicity time windows that clustered in the CAFS area, to better constrain the spatiotemporal evolution of the CAFS seismic cycle.

2.2. Coulomb stress transfer (CST) and fault modelling

We propose a novel approach to model seismogenic sources for CST calculation purposes, with the aim of reducing uncertainties on fault interaction. The cornerstone of this approach is adopting the hypothesis that the most reliable approximation of 2D fault geometry is an ellipse (Barnett *et al*., 1987; Walsh and Watterson, 1987; Gupta and Scholz, 2000). This concept is strictly related to the displacement variation that ranges from a maximum at the centre of the fault to zero at the elliptical tip-line loop. Furthermore, faults are commonly modelled as planar geometries in Coulomb calculations but, as demonstrated by Mildon *et al*. (2016), CST is highly sensitive to strike-variable geometries of receiver faults. Since a realistic CAFS-base model is of paramount importance in reducing calculation errors, we adopted a new strike-variable and ellipse-shaped 3D model as input file for the CST simulations.

For this purpose, we used the "3D Faults" code (Mildon *et al*., 2016) MATLAB code. To test the efficiency and the effective influence of this new model in terms of CST results, we performed calculations on planar-rectangular, strike-variable and elliptic faults. We used the same receiver and source faults but two different geometric models to find and quantify the differences.

We performed CST simulations within each seismic sequence, respecting the real rupture conditions of the earthquake (e.g. partial or entire rupture, slip distribution).

We conducted CST calculations assuming that, when an earthquake occurs on a fault, Coulomb stress can be transferred to the surrounding faults. The failure to do so will be promoted if the Coulomb stress change is positive, or it will be inhibited if it is negative (King *et al*., 1994). The change in Coulomb stress depends on the distance between the receiver fault and source fault, on their position, geometry, kinematics, and source fault slip. The CST was calculated with the following equation, using Coulomb 3.4 software (Lin and Stein, 2004; Toda *et al*., 2005):

$$\Delta CST = \Delta\tau s + \mu\Delta\sigma n \quad (2)$$

where ΔCST is the variation of the CST, $\Delta\tau s$ is the change of the shear stress, μ is the friction coefficient and $\Delta\sigma n$ is the change of the normal stress.

The input file was created by modelling the faults in the elastic half-space as linear elements with variable strike, dividing them into 0.5-kilometre long rectangular elements along the strike. The choice to use this very fine mesh as opposed to the usual use of kilometric mesh provides a precise evaluation of the variation in Coulomb stress by applying the various fault geometries, at the expense of the computational time employed. For this purpose, the use of the "3D Faults" code (Mildon *et al*., 2016) allowed generating 3D strike-variable faults from fault traces, and to create a slip distribution for each fault. Keeping the friction coefficient constant, we applied the code function that calculates the Coulomb stress for each individual rake, using the parameters specified in the input file for each of the rectangular elements forming the fault surface. Where possible, the actual earthquake slip was replicated by reproducing the coseismic slip distribution that occurred along the fault surface (only for recent earthquakes with a large amount of slip data). In turn, for the lesser-known earthquakes, a simple bull's-eye slip distribution, calibrated on the relative seismic moment released, was assumed, thus setting the location of maximum slip at the centre of the fault plane. When the width of the faults was not indicated in the examined bibliography, it was derived from standard geometric relationships (Gupta and Scholz, 2000) assuming a 1.5 aspect ratio (length/width). Conversely, for longer faults, the maximum fault depth was set to be equal to the thickness of the seismogenic layer [≈ 15 km: Gasparini *et al*. (1985) and Chiarabba and De Gori (2016)].

3. Results

3.1. The CAFS seismic cycle

The cumulative seismic moment released during the last 1,000 years was similar in the three main time windows separated by a time interval of circa 300-350 years, as hypothesised by Tondi and Cello (2003), who determined the seismic cycle using the calculation of the cumulative coseismic slip derived from the decomposition of the seismic moment. Alternatively, we directly used the cumulative seismic moment.

The graph in Fig. 1b shows how most of the seismic energy released in the last millennium can be associated with three distinct intervals: one between 1300 and 1400, one around 1700, and one from 1979 to 2016, corresponding to the latest events. Assuming that a millennium is a long enough time span to define the seismic cycle, it is possible to speculate that the time interval separating the release periods of most of the seismic energy is about 300-350 years. However, the quantity of energy released is not constant between the three time windows of seismicity. The seismic moment released by the first time window of seismicity is the highest (M_0 = 4.47E+26 dyne/cm), whereas the sum of the seismic moments released in the second and third time windows are 3.29E+26 dyne/cm and 1.93E+26 dyne/cm, respectively.

3.2. Fault modelling

The adoption of strike-variable and elliptic-shaped faults, in static CST modelling, revealed significant differences in terms of amount of transferred stress and stress patterns on the receiver faults, compared to the classic planar and rectangular faults. In particular, the ellipticity effect in the increasing lateral extension of the fault surfaces, to about half of their maximum depth, considerably reduces the distance between neighbouring faults, thus increasing the degree of interaction and, consequently, the amount of static Coulomb stress transferred to the

tips of the receiving faults located along the strike of the source faults (Fig. 2). Differences were also encountered in the stress pattern generated on laterally sub-parallel faults, subject to a larger decrease in stress. The intersection between the elliptical fault plane and the topographic surface defines the fault trace in map view, whereas the corresponding length is not the real fault length in depth, which, instead, is longer on average by 36.25% for ellipses with a geometric ratio of 3:2 between major and minor axis (Fig. 3). This consideration is consistent with the areal distribution of the instrumental hypocentres of the aftershocks and foreshocks that extend well beyond the tip of the causative fault, outlining, fairly precisely, the real extent of the fault in depth that roughly coincides with the modelling carried out.

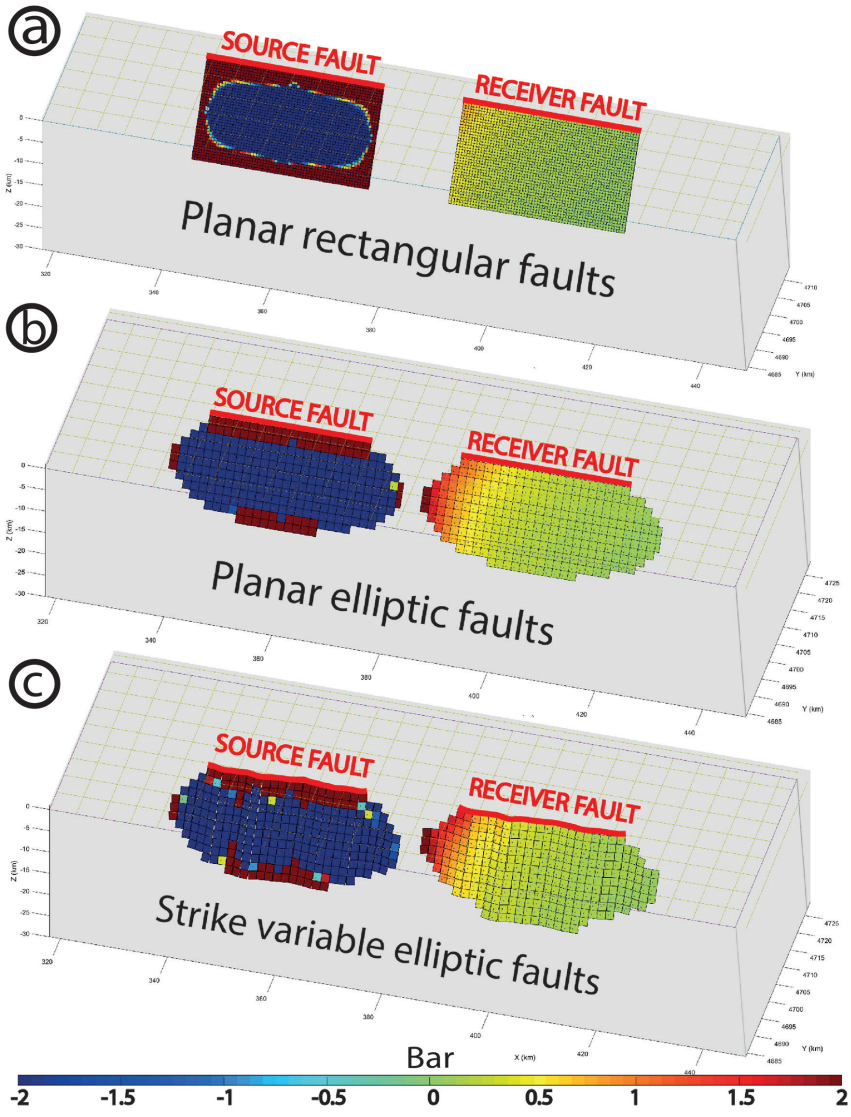

Fig. 2 - Simulations to test the influence of different fault models on CST. With a planar rectangular model (a), the receiver fault is negligibly influenced, whereas with elliptical faults the receiver fault tip shows higher stress values (b). By further adding the effect of the variable strike, a more heterogeneous stress pattern is noted on the receiver fault (c).

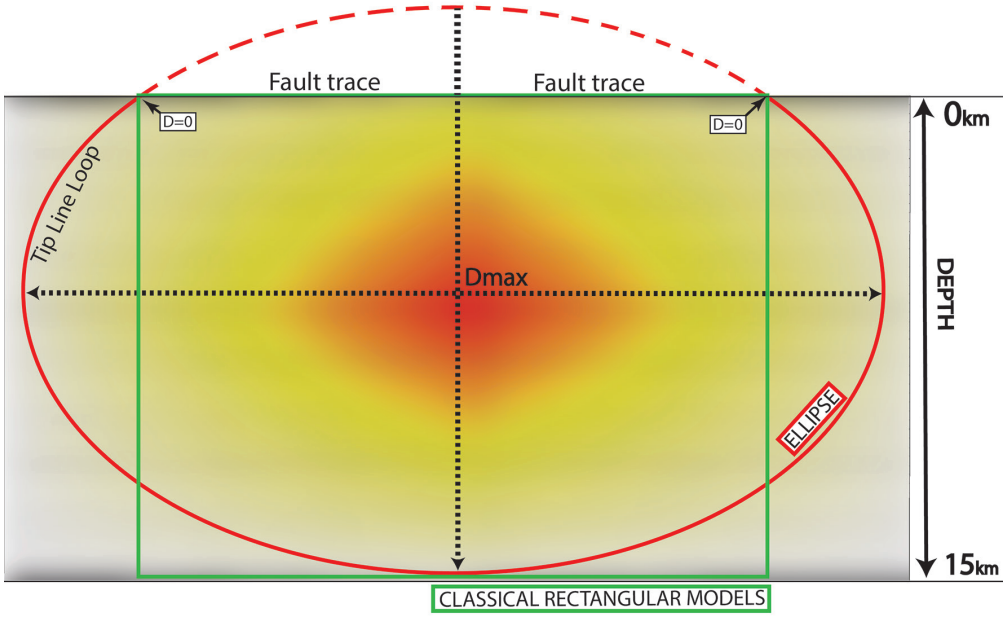

Fig. 3 - Comparison between the elliptical tip line loop of the fault (in red) and the commonly adopted rectangular shape (in green). The dashed part of the ellipse indicates the hypothetical continuation of the perimeter above the topographical surface. Centre-to-perimeter faded colours show the ideal displacement variation on the fault surface, that is maximum at the centre and zero along the tip line loop.

3.3. Coulomb stress transfer (CST)

The results regarding the CST modelling are encouraging, and highlight how this new methodology can make a significant difference compared to the classic methodology. The method was tested on several faults of some of the most interesting historical earthquakes, with the purpose of trying to understand how the surrounding faults were affected. A good agreement was found between the spatiotemporal evolution of the CAFS earthquake sequence and the permanent static stress transferred to the nearby faults. Faults falling into the stress shadows were inhibited in their reactivation after a strong earthquake was generated by the adjoining source fault. Conversely, fault segments, subject to increased stress, ruptured in shorter times than their characteristic return time, or the fault surfaces, partially affected by stress increase, subsequently showed partial ruptures only on the positively stressed fault tip. Some examples of the results obtained are given below.

3.3.1. Colfiorito 1279 versus Norcia 1328

The oldest earthquake considered in this work is that of 30 April 1279, which roughly struck the same area affected by the events of 1997. This sequence was sourced by the Colfiorito fault system, composed of two main structures (the Colfiorito North fault and Colfiorito South fault, CFFn and CFFs, respectively in Figs. 4 and 5), with an *en-echelon* geometrical relationship having a dextral step-over (Galli and Galadini, 1999). According to Galli and Galadini (1999), the 1279 earthquake is probably a twin of the 1997 one, and would have activated the same fault segments, corresponding in this work to the CFFn and CFFs. For such reasons, we modelled the simultaneous activation of both faults (Fig. 4c). The effect of the individual and contemporaneous activation

of the two segments were analysed in order to assess the CST for the following scenarios: i) CFFn as source fault (Fig. 4a); ii) CFFs as source fault (Fig. 4b); iii) simultaneous activation of both faults (Fig.4c). In all three cases, the magnitude of the event remained constant, and only the slip pattern was changed to adapt the magnitude to the different source faults.

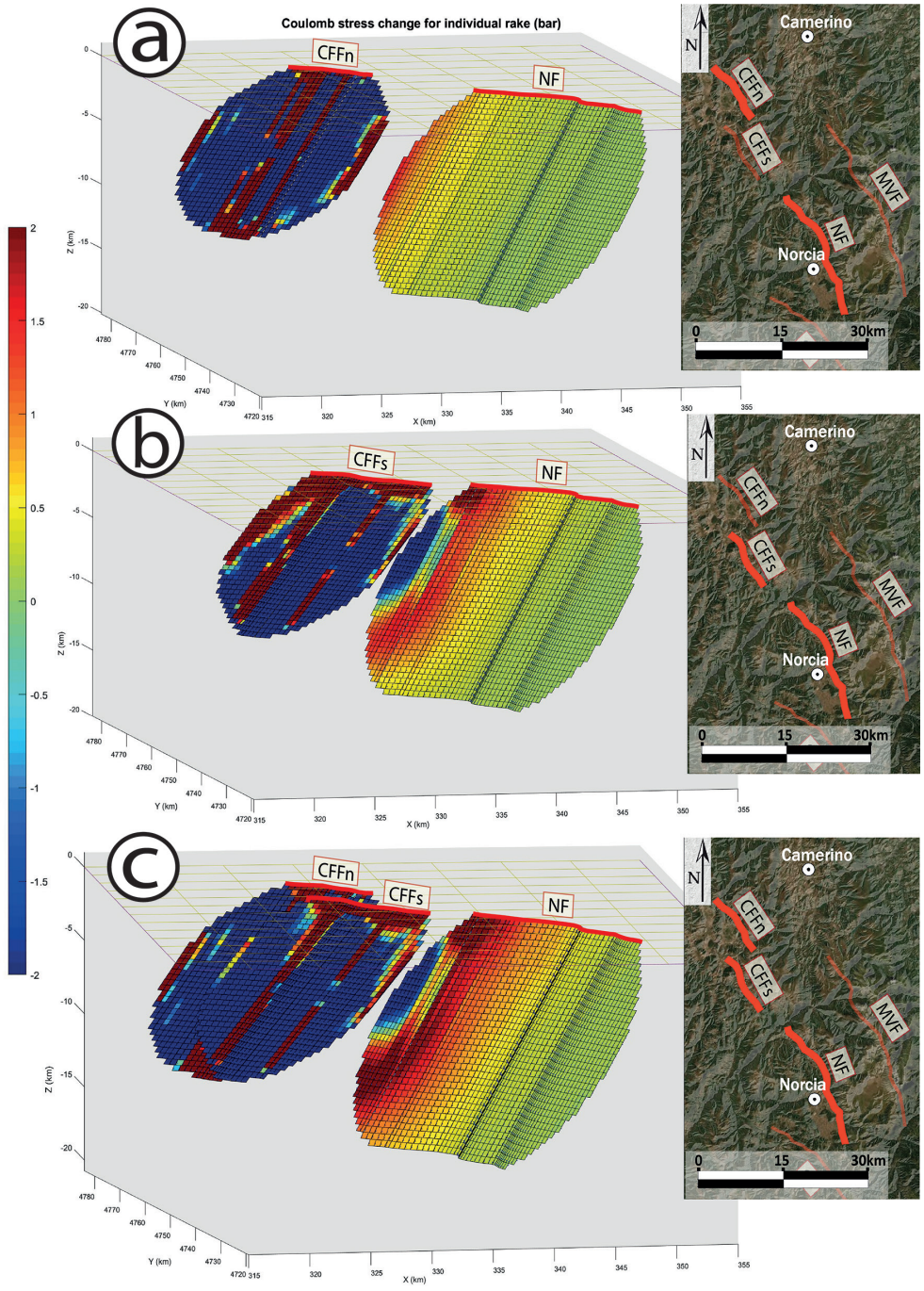

Fig. 4 - CST on the Norcia fault (NF) caused by the slip of the a) Colfiorito North fault (CFFn), b) Colfiorito South fault (CFFs) and c) simultaneous activation of both faults. The pictures on the right show the fault location in map view.

The receiver fault is the Norcia fault (NF), which subsequently activated in 1328. The aim is to understand the influence that the 1279 Colfiorito earthquake had on the NF in 1328.

The results of this calculation demonstrate how the mutual position of the faults influences the CST. The three faults, distributed from NW to SE along the same axis, sharing a similar strike, show fault tips very close to each other (Fig. 5). In the scenario, considering only the CFFn fault as the causative fault, only the northern tip of the NF would be positively loaded by the CST (Fig. 4a), with a stress increase of approximately 1.8 bar in a very small area. The slip on the CFFs fault, on the contrary, would have produced a more pronounced and heterogeneous CST pattern, partially influenced by the stress shadow area. In this case, in fact, the northern tip of the NF and the southern tip of the CFFs partially overlap at depth, creating a small zone of stress reduction in correspondence with the northern tip of the NF. The rest of the northern half of the receiver fault is positively stressed by a maximum of 2.2 bar. Ultimately, considering the simultaneous activation of the CFFn and CFFs (Figs. 4c and 5), the pattern, in the last case, is similar to the previous scenario, but with much higher CST values, even reaching 3 bar of positive stress in a large area.

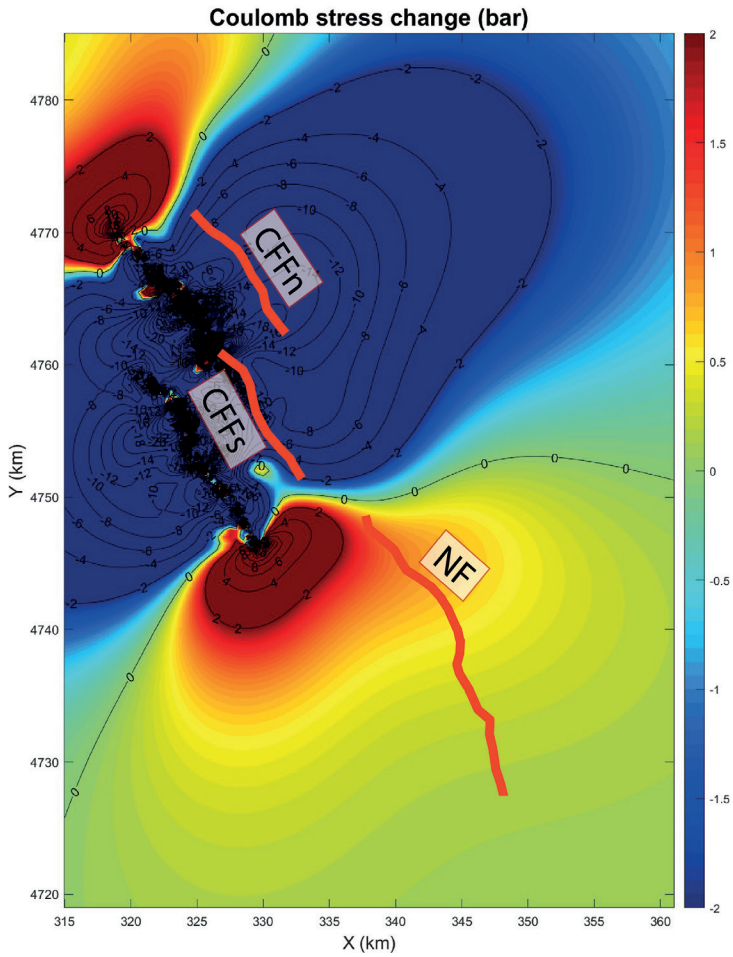

Fig. 5 - Map view of the spatial distribution of the CST caused by the simultaneous activation of the Colfiorito North and Colfiorito South faults. The calculation was performed on a plane at a 7.5-kilometre depth. Contour lines of equal stress variation on the receiver fault are drawn in black (numbers indicate stress in bar). The red traces represent the surface traces of the faults (CFFn - Colfiorito North fault, CFFs - Colfiorito South fault, NF - Norcia Fault).

3.3.2. Norcia 1328 versus Cascia 1599

In this case, the effect of the 1328 Norcia event (see Galli *et al*., 2005, 2018) on the Cascia fault system (Cascia plus Mt. Alvagnano faults), activated in 1599, i.e. 271 years later (Galli *et al*., 2019a), is calculated. On 4 December 1328, a M_w 6.5 earthquake struck an area between the Marche and Umbria regions, causing extensive damage and numerous casualties in Norcia. The distribution of the highest intensity data points suggests that part of the NF system was its causative structure (Galli *et al*., 2005, 2018). The eastern NF system borders the Quaternary Campi and Norcia basins, extending from NW to SE at surface, for about 23 km. Worthy of note is that in the late Middle Ages, the central Apennines underwent two additional earthquakes, which were rather far from Norcia: the first in 1349 in the Gran Sasso area (Galli *et al*., 2022a), and the second in 1461 on the Paganica fault (Chiarabba *et al*., 2009). The next earthquake occurred near Cascia, in 1599, with a M_w 6.0 (Galli *et al*., 2019a). This event attracted our attention as a possible candidate for the calculation of stress transfer for the following reasons:

i) the close proximity to the NF;
ii) the partial overlap between the tips of the two faults;
iii) the Cascia earthquake is located between two Norcia earthquakes (1328 and 1703), so it is possible to calculate the mutual stress transfer;
iv) the other two earthquakes, which occurred after 1328, struck an area very distant from Norcia, resulting in a negligible CST effect on the faults.

The Cascia fault system (i.e. the Cascia and Mt. Alvagnano faults) are over 19 km long, with a strike similar to the NF, and an overlapping step of about 5-10 km. The results of the CST from the NF to the Cascia fault (CF) during the 1328 earthquake are illustrated in Fig. 6. The causative fault undergoes an overall significant decrease in stress, except along vertical strips of the fault surface where there is a sudden change in strike, that is, along the fault bends. There, the CST increases by 2-6 bar, and a similar increase is also found in narrow portions of the northern and southern fault tips. The receiver fault undergoes a heterogeneous stress transfer pattern, with an evident negative stress lobe in its northern half, at a depth greater than 4 km. In this stress shadow zone, there is a decrease in stress up to 6 bar. The same amount of negative stress occurs at the centre of the fault but closer to the topographic surface, up to a depth of 2 km, while the remaining fault surface is subjected to a positive stress that reaches 2.5 bar. Furthermore, the CST pattern was modelled in map view at a 7.5-kilometre depth (Fig. 6), which corresponds to the most representative distribution of stress transfer in the surrounding area. Here, the two stress shadow lobes are much more extensive than the positively stressed ones.

3.3.3. Cascia 1599 versus Norcia 1703

We previously calculated the effect, in terms of CST, caused by the activation of the NF on the CF. Guided by the interest in modelling the opposite case, we modelled the 1599 earthquake (total seismic moment = 1.42E+25 dyne/cm; M_w 6.07) that occurred on the CF against the NF, which reactivated about a century later, in 1703, together with the CF (Galli *et al*., 2022b). This example is useful towards understanding whether there are differences between the receiver fault located in the hanging wall of the causative fault or the one located in the footwall. In fact, these two faults overlap for several kilometres, and both dip to the SW. The results of this calculation show the CF (causative) subject to negative stress except on the tips and in the superficial and deep extremes. This stress release is released in the surrounding crust and affects

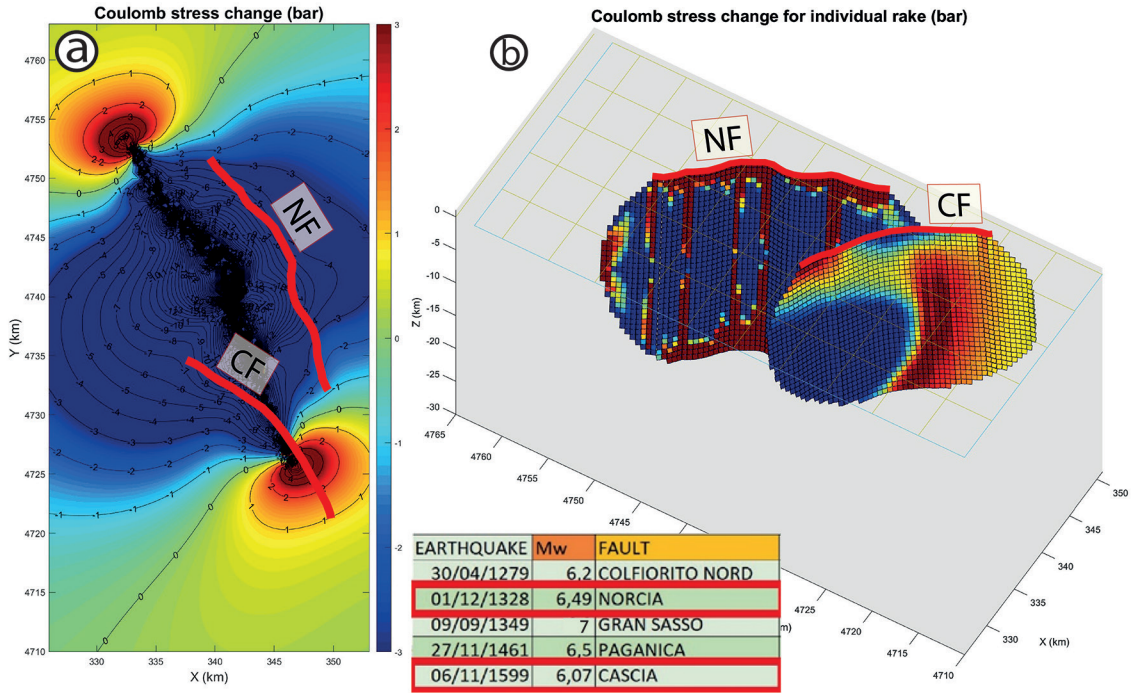

Fig. 6 - The CST on the Cascia fault (CF) following the 1328 M_w 6.49 seismic event caused by the slip on the Norcia fault (NF): a) plan view of the spatial distribution of CST on a plane at a 7.5-kilometre depth. Contour lines of equal stress variation on the receiver fault are drawn in black (numbers indicate stress in bar). The red traces represent the surface traces of the faults; b) 3D view of CST on fault surfaces.

the NF, especially at the bends. In Fig. 7, it is possible to observe how the red areas (positive stress) on the NF correspond to the bends, clearly visible in Fig. 7a. The zone covered by stress shadow is also clearly visible. It affects the overlapping zone of the two faults, and subtracts stress from the southern and superficial half of the NF. The northern tip, on the contrary, seems to have been negligibly affected by the reactivation of the CF.

4. Discussion

In this work, a new methodology to evaluate the interaction phenomena of neighbouring faults is applied to active faults of the central Apennines [CAFS in Cello *et al*. (1997)]. The choice of the aforementioned fault system is due to the good knowledge of the size, geometry and kinematics of the active faults, thanks to a considerable amount of available data, both geological (i.e. structural and paleoseismological) and seismological, the latter deriving from earthquakes, which occurred in recent decades (Rovida *et al*., 2022).

In the last 1,000 years, the area was subject to three major periods of seismic moment release [Fig. 1b, after Tondi and Cello (2003)]. The energy released during the first seismicity window (around 1300) was about 1.35 times greater than the second one, and 2.31 times greater than the third. This is consistent with the magnitude overestimation of historical earthquakes documented by Vannucci *et al*. (2021), likely linked to the intrinsic difficulties in estimating magnitude on the basis of macroseismic data. These uncertainties may lead to an overestimation of the seismic

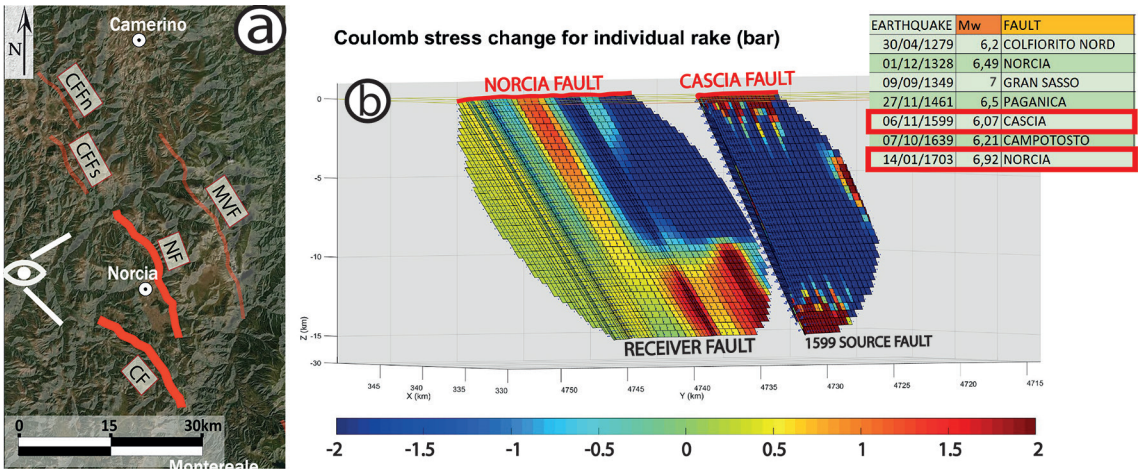

Fig. 7 - The CST on the Norcia fault (NF) following the 1599 M_W 6.07 seismic event caused by the slip on the Cascia fault (CF): a) map with the location of fault traces. The black eye is the point of view of Fig. 7b; b) 3D view of CST on fault surfaces.

moment generated by pre-instrumental events, therefore causing an imbalance between the three time windows of seismicity in the previous comparison of cumulative seismic moments. To minimise this issue, we subtracted the catalogue error, therefore aligning the data with more recent, and instrumentally recorded, events. By doing so, the estimation of the seismic moment for each sequence can be considered mutually comparable. The energy released during the last millennium has gradually decreased going from the first to the last seismicity window; the decrease stands at 1.18E+26 dyne/cm between the first and the second window, and 1.36E+26 dyne/cm between the second and the third. The difference in energy released between seismic periods also affects the correspondence between the depicted seismic cycle and the two dotted lines (i, ii), in Fig. 1b, that show the trend of a hypothetical seismic cycle, if it is energy (i) and time (ii) predictable. Considering the most recent seismic events of 2009 and 2016, and taking into account the error attributed to the moment magnitude of each selected instrumental and historical earthquake (Vannucci *et al.*, 2021), the CAFS seismic cycle seems to have lost the predictable character described by Tondi and Cello (2003). In hypothesising the possible causes that determined this heterogeneity between the three seismic cycle steps, worthy of consideration are the individual seismogenic sources belonging to the CAFS that released the greatest amount of energy in each of the three seismic windows. During the first seismic window, the energy released by the Gran Sasso fault system unequivocally dominates (Galli *et al.*, 2022a). The second seismic cycle step is largely taken up by the 1703 earthquake (M_W = 6.92), which involved the entire NF system (Tondi, 2000; Galli *et al.*, 2018). Ultimately, a large part of the seismic energy released during the last seismicity window is attributed to the Mt. Vettore fault (Villani *et al.*, 2018).

The intention to make the three-dimensional models of active faults more realistic has prompted reconsidering the simplifications assumed in previous modelling for calculating the CST. We tested a new model that, in addition to the variable strike, takes into consideration the elliptical shape of the faults in three dimensions. For the purpose of modelling, we considered a 3:2 ratio between the major axis and minor axis of the ellipse (Gupta and Scholz, 2000). This is a simplification that derives from the absence of reliable data on the areal extension in depth of the active faults analysed, but which seems to have a correspondence with the extension beyond the tips of the aftershocks and foreshocks. If we assume a fault aspect ratio (length/width) equal

to 1.5, the major axis of the ellipse is approximately 36.25% longer than the surface fault trace. This is consistent with the related aftershock distribution. Thus far, the elliptical shape of the fault was not considered in the CST calculations, and seems to be influential especially in loading or unloading the tip of the parallel faults.

This new fault geometry further affects the extent and shape of the stress shadow produced by the causative fault, which can impart negative stress to normal faults located across strikes, and can partially overlap the causative fault. The effect of the variable strike is appreciable when the bends are quite severe, creating a pattern with vertical bands more or less stressed than the surrounding areas. Mildon *et al*. (2016) demonstrated that alterations in the fault strike exert the most substantial influence on CST. A mere 10-20° shift in strike is adequate to elicit a change in stress, from positive to negative. It is noteworthy that the faults with the most significant stress discrepancies are those with prominent bends. However, if the positively stressed vertical bands occur on the causative fault surface, and it entirely ruptures without any partial activation, then, the stress accumulation bands should be deemed insignificant in triggering future earthquakes. Such behaviour is due to the fact that the rest of the fault surface has already dissipated all the previously accumulated stress, leaving narrow positive stress bands that are insufficient to cause a new main shock. Nevertheless, it would be of interest to explore the potential correlation between these positive stress zones and the occurrence of subsequent aftershocks, so as to confirm a possible relationship. However, the simplistic assumption remains that these bends continue in depth with the same geometry as on the surface. Another simplification concerns the slip pattern, which we have often assumed to have a bull's-eye shape due to the absence of slip data on historical earthquakes. In fact, we have noticed a large variation in stress imparted to the receiving faults as the slip pattern of the causative faults varies.

The influence of this new pseudorealistic model has been tested both on imaginary faults positioned in different spatial relationships, and on real faults, taking three historical earthquakes as examples (Colfiorito 1279, Norcia 1328, Cascia 1599). This new methodology has been applied, to these case studies, to test its feasibility, effectiveness and improvements, compared to the methodology used so far.

The CST calculation generated by the 1279 Colfiorito earthquake was also useful to develop the methodology for modelling two different faults with simultaneous activation. It is not certain whether both faults (CFFn and CFFs) contributed to the 1279 earthquake, however it is the more likely hypothesis, as argued by Galli and Galadini (1999). The analysis of the effect of the single activation of each of the two faults showed how neighbouring faults can be influenced in the event of a future activation of a single segment. The similarity between the stress pattern on the NF, after the activation of the CFFs alone and after the simultaneous activation of both CFFn and CFFs, is notable. With a conspicuous difference in the CST values, the latter (the CFFn and CFFS) show a much wider bar range, and a more limited stress shadow, while the positively stressed zone shows higher values. This proves the importance played by systems with *en-echelon* geometrical relationships, therefore by the partial overlapping of the tips, which, in the case of normal faults, generates a negative stress zone on the receiver fault.

This feature is also common to the second example analysed (1328 Norcia earthquake), where the stress shadow on the receiving fault (CF) is wider due to the greater overlapping area. Furthermore, the slip on the source fault is greater than the slip of the previous Colfiorito example, generating a much more accentuated stress reduction zone, with values reaching 6 bar. Although half of the CF seems to be impeded, 271 years later this structure generated an earthquake with an $M_W = 6$. This could be due to the long interval between the two earthquakes, which could have 'recharged' the fault with interseismic stress loading. Another theoretically-

acceptable explanation could be the splitting of the fault into two segments, the southern one called the Mount Alvagnano fault (MAF) in Galli *et al*. (2019a), and the northern one, the CF. Having two different strikes, these two segments accumulated stress differently: MAF stored positive stress and CF negative stress. Subsequently, in 1599, the southern segment (positively stressed) may have been activated, thus transmitting static and dynamic stress to the northern segment, consequently generating an instantaneous cascade effect.

In turn, the 1599 CF transferred Coulomb stress to the NF, but only in restricted and defined portions of the fault. The effect of the bends along the NF played a significant role in delimiting the positively stressed zones, while an extensive stress shadow is visible on the southern portion. This does not explain the massive reactivation of the NF during 1703, which also involved the Cascia segments [Cascia and Alvagnano faults in Galli *et al*. (2019a)], and the Upper Aterno Valley faults soon after. These multiple events could be the result of the combined action of static and dynamic stress transfer, but also of underground fluid migration or other factors influencing fault activity. In this case, in fact, the CST alone is not sufficient to justify the activation of so many structures.

In some cases, the link between CST and subsequent reactivation of the receiving fault (with positive stress change values) is not clear. Indeed, the variation in static stress is not the only influencing factor in the dynamics of fault activation, and other factors should be taken into consideration. Dynamic stress transfer, for instance, in the short term can affect after a rupture, due to the passage of seismic waves. However, what should certainly be implemented in the applicability of this methodology is also the calculation of the contribution of interseismic stress accumulation, controlled by the aseismic creep in the viscous lower crust.

5. Conclusions

In this work, the Tondi and Cello (2003) seismic cycle has been revised and updated in light of the most recent seismic events that struck the central Apennines in 2009 and 2016. Three time windows of seismicity have been identified, 300-350 years apart. A new methodology was, then, proposed to analyse the spatiotemporal evolution of seismicity, considering the contribution of CST on fault interactions. The aim was to create an innovative methodology capable of minimising simplifications in fault modelling. The introduction of an elliptical geometry of the faults studied resulted in huge changes in static stress transfer.

Specifically, three historical CAFS-related seismic events, Colfiorito 1279, Norcia 1328, and Cascia 1599, were examined to test this new methodology, which led to the following conclusions:

- the first simulation on the 1279 Colfiorito earthquake highlighted the importance of the position of the causative faults, with respect to the receiving fault, in building the stress pattern. The simultaneous activation of multiple segments increases the amount of stress transferred to the receiving fault, and yet has little influence on its pattern. The 1279 earthquake, according to the calculations of this work, promoted the subsequent reactivation of the NF, circa 50 years later;
- the second simulation, carried out on the NF activated in 1328, demonstrated that, in some cases, the classic CST is not a sufficient triggering factor. In such cases, the contribution of other additional factors, such as interseismic stress loading or dynamic coseismic stress transfer, could be considered influential. The CF, activated 271 years later, is, in fact, subjected to an extensive stress shadow that covers the northern half of the fault, while the southern one is positively stressed. The complete reactivation of this fault in 1599

could, therefore, be explained with the dynamic stress transfer from the southern to the northern portion during this seismic event, or with the change in the stress state of the fault during the interseismic period;

- the last simulation was performed on the NF, after the reactivation of the CF in 1599. It can be noted that the variable strike of the receiving fault has a marked influence on stress distribution, but this alone is not sufficient to explain the subsequent massive reactivation of the Norcia, Cascia, and part of the Upper Aterno Valley faults in 1703. Therefore, other mechanisms, not considered in this work, may have played a leading role.

The efficiency of this novel approach to the analysis of the seismic cycle, and the influence of static CST have been tested on historical seismic activities. The workflow presented may be adopted in future advanced applications for estimating active fault rupture susceptibility, feasibly integrating additional multidisciplinary data from research branches that study other factors, which may influence fault activity (e.g. fluid pressure, regional stress, interseismic stress accumulation in the viscous lower crust, etc.). Important implications of this new methodology are desirable in the context of seismic hazard assessment for the implementation of advanced and integrated seismic risk reduction strategies and disaster management.

Acknowledgments. We would like to acknowledge Zoë Mildon and Manuel-Lukas Diercks for their kind assistance in using the "3D Faults" MATLAB code. This work was supported by the FAR Unicam project, "Novel Approach for Seismic Hazard Analysis-NoHard'', supervised by Emanuele Tondi.

REFERENCES

Aki K. and Richards P.G.; 1980: *Quantitative Seismology, 2nd ed*. J. Ellis, University Sciences Books, New York, NY, USA, 700 pp.

Amato A., Azzara R., Chiarabba C., Cimini G.B., Cocco M., Di Bona M., Margheriti L., Mele F., Selvaggi G., Basili A., Boschi E., Courbolex F., Deschamps A., Gaffet S., Bittarelli G., Chiaraluce L., Piccinini D. and Ripepe M.; 1998: *The 1997 Umbria-Marche, Italy, earthquake sequence: a first look at the main shocks and aftershocks*. Geophys. Res. Lett., 25, 2861-2864.

Barchi M., Galadini F., Lavecchia G., Messina P., Michetti A.M., Peruzza L., Pizzi A., Tondi E. and Vittori E.; 2000: *Sintesi delle conoscenze sulle faglie attive in Italia Centrale: parametrizzazione ai fini della caratterizzazione della pericolosità sismica.* CNR-Gruppo Nazionale per la Difesa dai Terremoti, Roma, Italy, 62 pp.

Barnett J.A., Mortimer J., Rippon J.H., Walsh J.J. and Watterson J.; 1987: *Displacement geometry in the volume containing a single normal fault*. AAPG Bull., 71, 925-937.

Brodsky E.E. and van der Elst N.J.; 2014: *The uses of dynamic earthquake triggering*. Annu. Rev. Earth Planet. Sci., 42, 317-339, doi: 10.1146/annurev-earth-060313-054648.

Cello G., Mazzoli S., Tondi E. and Turco E.; 1997: *Active tectonics in the central Apennines and possible implications for seismic hazard analysis in peninsular Italy*. Tectonophys., 272, 43-68.

Cello G., Deiana G., Mangano P., Mazzoli S., Tondi E., Ferreli L., Maschio L., Michetti A.M., Serva L. and Vittori E.; 1998: *Evidence for surface faulting during the September 26, 1997, Colfiorito (central Italy) earthquakes*. J. Earthquake Eng., 2, 303-324.

Chiarabba C. and De Gori P.; 2016: *The seismogenic thickness in Italy: constraints on potential magnitude and seismic hazard*. Terra Nova, 28, 402-408.

Chiarabba C., Amato A., Anselmi M., Baccheschi P., Bianchi I., Cattaneo M., Cecere G., Chiaraluce L., Ciaccio M.G., De Gori P., De Luca G., Di Bona M., Di Stefano R., Faenza L., Govoni A., Improta L., Lucente F.P., Marchetti A., Margheriti L., Mele F., Michelini A., Monachesi G., Moretti M., Pastori M., Piana Agostinetti N., Piccinini D., Roselli P., Seccia D. and Valoroso L.; 2009: *The 2009 L'Aquila (central Italy) Mw 6.3 earthquake: main shock and aftershocks*. Geophys. Res. Lett.: Solid Earth, 36, L18308, 6 pp., doi: 10.1029/2009GL039627.

Chiaraluce L., Valoroso L., Piccinini D., Di Stefano R. and De Gori P.; 2011: *The anatomy of the 2009 L'Aquila normal fault system (central Italy) imaged by high resolution foreshock and aftershock locations*. J. Geophys. Res.: Solid Earth, 116, B12311, 25 pp., doi: 10.1029/2011JB008352.

Chiaraluce L., Di Stefano R., Tinti E., Scognamiglio L., Michele M., Casarotti E., Cattaneo M., De Gori P., Chiarabba C., Monachesi G., Lombardi A., Valoroso L., Latorre D. and Marzorati S.; 2017: *The 2016 central Italy seismic sequence: a first look at the mainshocks, aftershocks, and source models*. Seismol. Res. Lett., 88, 757-771.

Galadini F. and Galli P.; 2000: *Active tectonics in the central Apennines (Italy) - input data for seismic hazard assessment.* Nat. Hazards, 22, 225-268, doi: 10.1023/A:1008149531980.

Galadini F. and Messina P.; 2001: *Plio-Quaternary changes of the normal fault architecture in the central Apennines (Italy)*. Geodinamica Acta, 14, 321-344.

Galderisi A. and Galli P.; 2020: *Coulomb stress transfer between parallel faults. The case of Norcia and Mt. Vettore normal faults (Italy, 2016 Mw 6.6 earthquake)*. Results Geophys. Sci., 1, 100003, 8 pp., doi: 10.1016/j.ringps.2020.100003.

Galli P.; 2020: *Recurrence times of central-southern Apennine faults (Italy): hints from palaeoseismology*. Terra Nova, 32, 399-407.

Galli P. and Galadini F.; 1999: *Seismotectonic framework of the 1997-98 Umbria-Marche (central Italy) earthquakes.* Seismol. Res. Lett., 70, 404-414.

Galli P., Galadini F. and Calzoni F.; 2005: *Surface faulting in Norcia (central Italy): a "paleoseismological perspective"*. Tectonophys., 403, 117-130.

Galli P., Galadini F. and Pantosti D.; 2008: *Twenty years of paleoseismology in Italy*. Earth Sci. Rev., 88, 89-117.

Galli P., Giaccio B., Messina P., Peronace E. and Zuppi G.M.; 2011: *Palaeoseismology of the L'Aquila faults (central Italy, 2009, Mw 6.3 earthquake): implications for active fault linkage*. Geophys. J. Int., 187, 1119-1134.

Galli P., Peronace E., Bramerini F., Castenetto S., Naso G., Cassone F. and Pallone F.; 2016: *The MCS intensity distribution of the devastating 24 August 2016 earthquake in central Italy (MW 6.2)*. Ann. Geophys., 59, 19 pp., doi: 10.4401/ag-7287.

Galli P., Galderisi A., Ilardo I., Piscitelli S., Scionti V., Bellanova J. and Calzoni F.; 2018: *Holocene paleoseismology of the Norcia Fault system (central Italy).* Tectonophys., 745, 154-169.

Galli P., Galderisi A., Marinelli R., Peronace E., Messina P. and Polpetta F.; 2019a: *A reappraisal of the 1599 earthquake in Cascia (Italian central Apennines): hypothesis on the seismogenic source.* Tectonophys., 774, 228287, 15 pp., doi: 10.1016/j.tecto.2019.228287.

Galli P., Galderisi A., Peronace E., Giaccio B., Hajdas I., Messina P., Pileggi D. and Polpetta F.; 2019b: *The awakening of the dormant Mount Vettore Fault (2016 central Italy earthquake, Mw 6.6): paleoseismic clues on its millennial silences*. Tectonics, 38, 687-705.

Galli P., Galderisi A., Messina P. and Peronace E.; 2022a: *The Gran Sasso fault system: paleoseismological constraints on the catastrophic 1349 earthquake in central Italy*. Tectonophys., 822, 229156, 29 pp., doi: 10.1016/j.tecto.2021.229156.

Galli P., Peronace E. and Messina P.; 2022b: *Archaeoseismic evidence of surface faulting in 1703 Norcia earthquake (central Italian Apennines, Mw 6.9)*. Geosci., 12, 14, 13 pp., doi: 10.3390/geosciences12010014.

Gasparini C., Iannaccone G. and Scarpa R.; 1985: *Fault-plane solutions and seismicity of the Italian peninsula*. Tectonophys., 117, 59-78.

Gold R.D., Cowgill E., Arrowsmith J.R. and Friedrich A.M.; 2017: *Pulsed strain release on the Altyn Tagh Fault, northwest China*. Earth Planet. Sci. Lett., 459, 291-300, doi: 10.1016/j.epsl.2016.11.024.

Gomberg J. and Johnson P.; 2005: *Dynamic triggering of earthquakes*. Nature, 437, 830, doi: 10.1038/437830a.

Gupta A. and Scholz C.H.; 2000: *A model of normal fault interaction based on observations and theory*. J. Struct. Geol., 22, 865-879.

Hanks T.C. and Kanamori H.; 1979: *A moment magnitude scale.* J. Geophys. Res.: Solid Earth, 84, 2348-2350.

Hetzel R. and Hampel A.; 2005: *Slip rate variations on normal faults during glacial-interglacial changes in surface loads*. Nature, 435, 81-84, doi: 10.1038/nature03562.

ISIDe Working Group; 2007: *Italian seismological instrumental and parametric database (ISIDe)*. Istituto Nazionale di Geofisica e Vulcanologia (INGV), doi: 10.13127/ISIDE.

King G.C., Stein R.S. and Lin J.; 1994: *Static stress changes and the triggering of earthquakes*. Bull. Seismol. Soc. Am., 84, 935-953.

Lin J. and Stein R.S.; 2004: *Stress triggering in thrust and subduction earthquakes and stress interaction between the southern San Andreas and nearby thrust and strike-slip faults*. J. Geophys. Res. B: Solid Earth, 109, 19 pp., doi: 10.1029/2003JB002607.

Messina P., Galadini F., Galli P. and Sposato A.; 2002: *Quaternary basin evolution and present tectonic regime in the area of the 1997-1998 Umbria-Marche seismic sequence (central Italy)*. Geomorphol., 42, 97-116.

Mildon Z.K., Toda S., Faure Walker J.P. and Roberts G.P.; 2016: *Evaluating models of Coulomb stress transfer: is variable fault geometry important?*. Geophys. Res. Lett., 43, 12407-12414, doi: 10.1002/2016GL071128.

Oskin M., Perg L., Shelef E., Strane M., Gurney E., Singer B. and Zhang X.; 2008: *Elevated shear zone loading rate during an earthquake cluster in eastern California*. Geol., 36, 507-510, doi: 10.1130/G24814A.1.

Pantosti D. and Boncio P.; 2012: *Understanding the April 6th, 2009 L'Aquila earthquake-the geological contribution: an introductory note to the special issue*. Ital. J. Geosci., 131, 303-308.

Rovida A., Locati M., Camassi R., Lolli B., Gasperini P. and Antonucci A.; 2022: *Catalogo Parametrico dei Terremoti Italiani CPTI15, versione 4.0.* Istituto Nazionale di Geofisica e Vulcanologia (INGV), Roma, Italy, doi: 10.13127/cpti/cpti15.4.

Shimazaki K. and Nakata T.; 1980: *Time-predictable recurrence model for large earthquakes.* Geophys. Res. Lett., 7, 279-282.

Toda S., Stein R.S., Richards-Dinger K. and Bozkurt S.B.; 2005: *Forecasting the evolution of seismicity in southern California: animations built on earthquake stress transfer*. J. Geophys. Res. B: Solid Earth, 110, B05S16, 17 pp., doi: 10.1029/2004JB003415.

Toda S., Stein R.S., Beroza G.C. and Marsan D.; 2012: *Aftershocks halted by static stress shadows*. Nature Geosci., 5, 410-413.

Tondi E.; 2000: *Geological analysis and seismic hazard in the central Apennines (Italy)*. J. Geodyn., 29, 517-533.

Tondi E. and Cello G.; 2003: *Spatiotemporal evolution of the central Apennines fault system (Italy)*. J. Geodyn., 36, 113-128.

Tondi E., Jablonská D., Volatili T., Michele M., Mazzoli S. and Pierantoni P.P.; 2020: *The Campotosto linkage fault zone between the 2009 and 2016 seismic sequences of central Italy: implications for seismic hazard analysis*. Geol. Soc. Am. Bull., 133, 1679-1694, doi: 10.1130/B35788.1.

Vannoli P., Burrato P., Fracassi U. and Valensise G.; 2012: *A fresh look at the seismotectonics of the Abruzzi (central Apennines) following the 6 April 2009 L'Aquila earthquake (Mw 6.3)*. Ital. J. Geosci., 131, 309-329.

Vannucci G., Lolli B. and Gasperini P.; 2021: *Inhomogeneity of macroseismic intensities in Italy and consequences for macroseismic magnitude estimation*. Seismol. Res. Lett., 92, 2234-2244.

Velasco A.A., Hernandez S., Parsons T.O.M. and Pankow K.; 2008: *Global ubiquity of dynamic earthquake triggering*. Nature Geosci., 1, 375-379.

Villani F., Pucci S., Civico R., De Martini P.M., Cinti F.R. and Pantosti D.; 2018: *Surface faulting of the 30 October 2016 Mw 6.5 central Italy earthquake: detailed analysis of a complex coseismic rupture*. Tectonics, 37, 3378-3410.

Vittori E., Deiana G., Esposito E., Ferreli L., Marchegiani L., Mastrolorenzo G., Michetti A.M., Porfido S., Serva L., Simonelli A.L. and Tondi E.; 2000: *Ground effects and surface faulting in the September-October 1997 Umbria-Marche (central Italy) seismic sequence*. J. Geodyn., 29, 535-564.

Walsh J.J. and Watterson J.; 1987: *Distributions of cumulative displacement and seismic slip on a single normal fault surface*. J. Struct. Geol., 9, 1039-1046.

Wedmore L.N.J., Faure Walker J.P., Roberts G.P., Sammonds P.R., McCaffrey K.J.W. and Cowie P.A.; 2017: *A 667 year record of coseismic and interseismic Coulomb stress changes in central Italy reveals the role of fault interaction in controlling irregular earthquake recurrence intervals*. J. Geophys. Res.: Solid Earth, 122, 5691-5711.

Corresponding author: Giorgio Valentini
School of Science and Technology, Geology Division, University of Camerino
Via Gentile III da Varano 7, 62032 Camerino (MC), Italy
Phone: +39 347 4363676; e-mail: giorgio.valentini@unicam.it